Selective Electrochemical Reductive Amination of Benzaldehyde at Heterogeneous Metal Surfaces

Zachary J Schiffer,[1] Minju Chung,[1] Katherine Steinberg,[1] and Karthish Manthiram [*,1]

[1]Department of Chemical Engineering, Massachusetts Institute of Technology, 77 Massachusetts Avenue, Cambridge, MA 02139

*Corresponding author, Email: karthish@mit.edu

Abstract

Ammonia is one of the largest volume commodity chemicals, and electrochemical routes to ammonia utilization are appealing due to increasingly available renewable electricity. In this work, we demonstrate an electrochemical analogue to reductive amination for the synthesis of benzylamine from benzaldehyde and ammonia. Previous works on electrochemical reductive amination generally focus on proof-of-concept outer-sphere routes. We demonstrate an inner-sphere route, opening a large phase space of heterogeneous electrocatalysts that can direct selectivity and drive the reaction. In our system, imine hydrogenation proceeds on a silver electrocatalyst at ambient conditions in methanol with an initial Faradaic efficiency toward the primary amine product of ~80% and partial current greater than 4 mA/cm^2 at -1.96 V vs. Fc/Fc$^+$ (-1.36 V vs. NHE). Silver was selected after evaluating diverse transition metal electrocatalysts, and with density functional theory, we found that the reaction rate on various metals is best described by the charge density distribution above the metal surface, independent of molecular adsorption energies. On silver, the catalyst that promotes amination with the highest Faradaic efficiency and one of the highest partial currents, the rate-determining step was found to be the

initial electron transfer to the imine. Overall, this work on the kinetics of electrochemical reductive amination represents a step toward inner-sphere electrochemical reductive amination systems for the synthesis of amines that currently rely on thermochemical reductive amination.

Introduction

In addition to being one of the largest volume commodity chemicals, ammonia is also a ubiquitous nitrogen precursor throughout the chemical industry.[1] Nitrogen functionality in polymers, pharmaceuticals, and specialty chemicals can often be traced back to either ammonia or reagents that are produced from ammonia (Figure 1, left). Decarbonized production of green ammonia itself is gaining momentum; ammonia can be synthesized sustainably using renewable electricity, nitrogen, and water, either indirectly via traditional Haber-Bosch fed with hydrogen gas produced from water splitting, or directly via an electrochemical Haber-Bosch process.[2–4] This provides motivation for also electrifying the downstream steps in which ammonia is utilized in chemical synthesis. At present, chemical syntheses involving ammonia rely on temperature and pressure as driving forces, and they often contain multiple steps and separations before achieving the desired product (Figure 1, left). As renewable electricity becomes increasingly affordable and accessible, however, there is an opportunity to rethink these chemical processes which utilize ammonia, potentially reducing carbon footprints and enabling distributed chemical synthesis through the implementation of analogous electrochemical processes.[5–9] Specifically, green ammonia can be electrochemically reacted with other renewable resources to form desired nitrogen containing products with only ca. 1 V of applied potential (Figure 1, right).

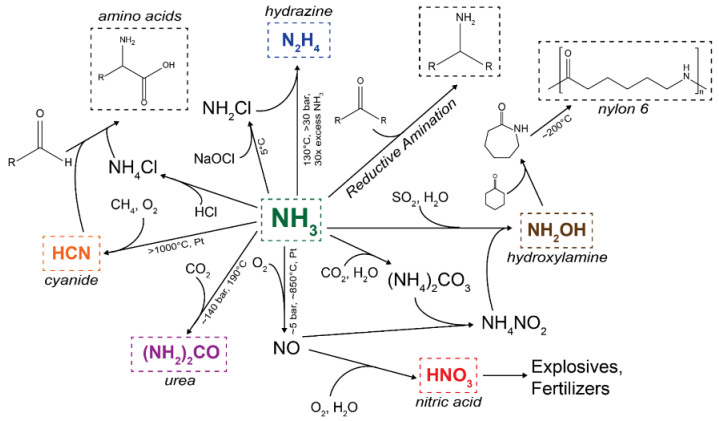

Reaction	E^0 (V)
$\frac{1}{2}N_2 + \frac{3}{2}H_2O \rightarrow NH_3 + \frac{3}{4}O_2$	-1.1
$NH_3 \rightarrow \frac{1}{2}N_2H_4 + \frac{1}{2}H_2$	-1.0
$NH_3 + H_2O \rightarrow NH_2OH + H_2$	-1.3
$NH_3 + 3H_2O \rightarrow HNO_3 + 4H_2$	-0.8
$NH_3 + \frac{1}{2}CO_2 \rightarrow \frac{1}{2}(NH_2)_2CO + \frac{1}{4}O_2 + \frac{1}{2}H_2$	-1.9
$NH_3 + CH_4 \rightarrow HCN + 3H_2$	-0.3
$NH_3 +$ 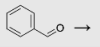 $\rightarrow$ 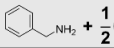 $+ \frac{1}{2}O_2$	-1.0

Figure 1. Web of chemicals industrially synthesized from ammonia. Ammonia is a nexus molecule, responsible for nitrogen functionality in many important molecules either directly or indirectly (left). Note that the processes depicted are simplified and are intended to qualitatively show the steps and reactants involved, not exhaustively depict the various synthetic pathways (See Supplementary Data Analysis section for more details on these routes). Instead of using temperature and pressure to drive reactions, one can instead drive the same reactions depictured in the web electrochemically (table on right) using renewable resources (e.g., water and sunlight). Thermodynamically, these reactions requires ca. 1 V to drive, an accessible amount. The first row of the table shows how ammonia itself can be made using renewable electricity. The bottom row depicts the overall reaction studied in this work. Note that all reactions are in the gas phase for simplicity. More details on equilibrium potential calculations given in Tables S3 and S4.

The electrochemical utilization of ammonia in chemical synthesis using renewable energy sources will act to further increase the interconnectedness of the chemical and energy industries, especially since ammonia is a serious contender as a chemical carrier of renewable electricity [7].

One of the most versatile and industrially relevant thermochemical methods to utilize ammonia and form carbon-nitrogen bonds is reductive amination.[10–15] Reductive amination involves two steps: (1) the reaction of ammonia (or an amine) with a carbonyl group to form an imine; and (2) the reduction of the imine to form a carbon-nitrogen single bond. The formation of the imine is an equilibrium step that can sometimes occur spontaneously at ambient conditions

but can also be aided by removal of water (a product). The imine reduction can rely on heterogeneous catalysts (e.g., hydrogen gas and palladium metal)[11,12,14], homogeneous catalysts (e.g., hydrogen gas and rhodium or ruthenium complexes)[14,16,17], or stoichiometric reductants such as sodium borohydride[11,18]. In the catalytic cases where hydrogen gas is the reductant, elevated temperatures and pressures are often used to drive the reduction step.[12,14,15] In the case of many stoichiometric reductants, the reduction results in undesirable stoichiometric byproducts which increase overall reaction costs and complexity as well as chemical waste and environmental impact.

We focus on the specific reaction of benzaldehyde with ammonia to form benzylamine. Benzylamine is a useful reagent in a variety of organic syntheses, including as an intermediate in production of pharmaceuticals and surface coatings[19] The synthesis of benzylamine offers an ideal platform for studying new reductive amination processes because the benzylimine intermediate is stable (i.e., it is favored at ambient conditions in non-aqueous solvents and there is no keto-enol tautomerization), meaning we can be confident we are studying the hydrogenation of a carbon-nitrogen double bond. Current methods for the synthesis of benzylamine include reductive amination with heterogeneous catalysts (e.g. Raney Nickel[20], Co[21], Ni[22], and Pd[23], to name a few) and reductive amination via ruthenium or rhodium complexes.[16,17] In these cases, the reaction is generally conducted at elevated temperatures (> 80°C) and elevated pressures (>20 bar H2) (Figure 2).

Other industrial routes to synthesize benzylamine include the reaction of benzyl chloride with ammonia or the reduction of benzonitrile, yet these routes involve additional reactions and hazardous chemicals, and they are not as generalizable as reductive amination.[20] Here, we explore how reductive amination for the synthesis of benzylamine can be driven using an applied electrical voltage instead of pressure and temperature, a so-called electrochemical reductive amination (ERA) reaction. As with other electrochemical reactions to utilize ammonia, ERA of

benzaldehyde theoretically only requires ca. 1 V of applied potential (Figure 1, right; more details in Tables S3 and S4).

Thermochemical reductive amination, particularly in the case of benzylamine synthesis, has been extensively studied.[14,15,21–23] Previous research on ERA, however, has generally focused on outer sphere reactions (e.g., with glassy carbon or mercury electrodes) and proof-of-concept experiments limited to cyclic voltammograms and generally secondary amine products.[24–32] Some previous studies have explored inner-sphere synthesis of secondary amines on metal catalysts (i.e., on Cu, Zn, Sn, and Ag electrodes)[33] or reduction of nitrile groups to primary amines (on Raney nickel) [34], but these studies have been limited in their exploration of the influence of catalysts and reaction conditions and do not generally discuss ERA for the synthesis of primary amines (more detailed comparison of previous works in Table S2). Electrochemical reduction of nitro functional groups to amino functional groups using water as a hydrogen source has also been studied.[35]

In general, electrochemical reactions can proceed via outer-sphere mechanisms, in which the reactants approach an electrode surface but do not form a chemical bond with a catalyst, or via inner-sphere mechanisms, which involve the reactants binding to the electrode surface with a chemical bond.[36] Outer-sphere reactions have little to no dependence on the catalyst material and can be driven with electrodes that do not form a bond with reactants; glassy carbon (GC) and mercury electrodes are commonly used electrodes for outer-sphere reactions. To alter the reactivity of an outer-sphere reaction, one must primarily alter the reaction environment by changing the solvent or incorporating additives in the solution. On the other hand, inner-sphere reactions depend more intimately on the catalyst material due to the formation of chemical bonds with reaction intermediates.

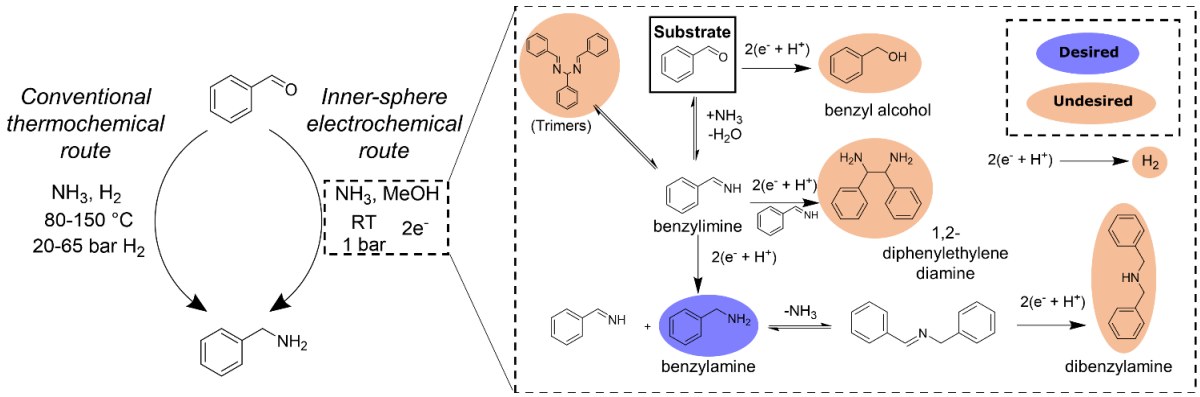

Figure 2. Overview of the system and relevant reactions. Conversion from benzaldehyde to benzylamine can occur thermochemically at elevated temperatures or pressures (left) or electrochemically at ambient conditions with an applied voltage and heterogeneous catalyst (right). During electrochemical reductive amination of benzaldehyde, the benzaldehyde first forms benzylimine, which can then be reduced to benzylamine (blue oval). At each step of the process, side reactions can produce undesired products including benzyl alcohol, dibenzylamine, 1,2-diphenylethylenediamine, hydrobenzamide, and hydrogen gas (orange ovals).

This means that reactivity can be controlled by tuning the catalyst composition or morphology. Inner-sphere reactions are often advantageous because of the large phase space catalytic materials offer to guide selectivity in a reaction, yet heterogeneous electro-organic syntheses, particularly in the case of ERA, often rely on outer-sphere mechanisms.

Recent research on biomass upgrading has many examples of inner-sphere electrochemical reduction of benzaldehyde and furfural, providing a starting point to our work.[37–50] These studies have found that electrochemical aldehyde reductions have a strong dependence on catalyst metal, solvent, and potential. In many ways, these systems are analogous to electrochemical benzylimine reduction.

In this work, we demonstrate ERA for the synthesis of benzylamine in a non-aqueous environment. This model reaction enables us to study and characterize an inner-sphere route of ERA for a useful primary amine synthesis. We show that the ERA of benzaldehyde is inner-sphere and that trends in reactivity can be best interpreted using a descriptor that is dependent on the electronic structure of the catalyst itself, not a particular binding energy as is traditionally used to describe reactivity trends. In addition, we explore the influence of potential and reactant

concentrations on the system, finding that the rate-determining step is likely the initial electron transfer to the benzylimine. We also observe a decay in reaction rate and Faradaic efficiency as conversion increases, possibly indicating undesirable side reactions that lead to poisoning or fouling of the catalyst during operation.

Results and Discussion

The synthesis of benzylamine from benzaldehyde and ammonia is a multi-step reaction with several paths to undesired side products (Figure 2). The first step of this reaction is the formation of the imine from the starting benzaldehyde substrate (box labeled “Substrate”, top of Figure 2). By allowing for the reaction of all benzaldehyde before applying a potential (confirmed via NMR, Figure S4), we have removed the likelihood of benzaldehyde reduction to benzyl alcohol (orange oval at top, Figure 2). Only trace amounts of benzyl alcohol product are sometimes observed in the electrolyte post electrolysis. Once the imine has formed, there are a few possible reaction paths. The first is an undesirable equilibrium involving multiple imines forming trimers in solution such as hydrobenzamide (orange oval, top left of Figure 2).[16,51] The desired pathway is the reaction of the imine with electrons and protons directly to form benzylamine (blue oval, Figure 2). In addition to this desired reaction, two imines can couple to form a diamine product, 1,2-diphenylethylenediamine (orange oval in center, Figure 2), a process that likely proceeds through an outer-sphere radical coupling mechanism.[44] Once the primary amine is formed, it can further react with an unreacted primary imine to form a secondary imine, which can be reduced to a secondary amine product, dibenzylamine (orange oval in bottom right corner, Figure 2). We seek to encourage formation of the desired benzylamine and suppress the formation of these other

side products through identification of a suitable catalyst.

During electrolysis, the Pt counter electrode in this system is likely oxidizing methanol or polymerizing the substrate (generating a yellow film observed on foil). To increase sustainability of the overall reaction, water could be oxidized at the anode, resulting in the overall reaction shown at the bottom of the table in Figure 1, but this is beyond the scope of the current work and does not influence the cathode reactions.

Inner-Sphere Mechanism

As mentioned previously, most research on ERA has focused on outer-sphere routes.[24–32] However, in the case of ERA for the synthesis of benzylamine using methanol as a solvent, we find that there is, in fact, a dependence of the reaction kinetics on the electrode material (Figure 3). In particular, the partial current at -1.9 V vs. Fc/Fc^+ (ca. -1.3 V vs. NHE[52]) toward the primary amine product on glassy carbon (expected to represent an outer-sphere mechanism) is less than 0.2 mA/cm^2 and the Faradaic efficiency is less than 25% toward the primary amine (top, Figure 3).

Ten metal foils were compared, and the partial currents ranged from ~0.5 mA/cm^2 for Pt and Zn to ~4.3 mA/cm^2 for Pd (brief discussion of comparison to thermochemical rate constant in Supplementary Data Analysis section), while the Faradaic efficiencies ranged from less than ~2% for Pt to greater than ~75% for Ag (Figure 3). This wide range of partial currents and Faradaic efficiencies indicates that the reaction has a strong metal dependence, suggesting that the reaction is proceeding through an inner-sphere mechanism.

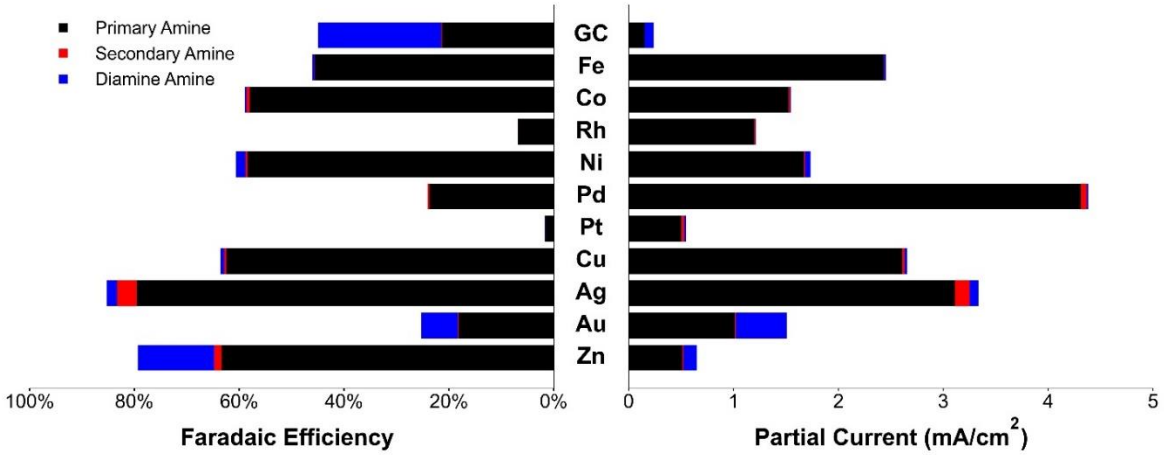

Figure 3. Metal dependence of Faradaic efficiency (left) and partial current (right) toward various amine products. All tests involved a 1 M tetrabutylammonium tetrafluoroborate (TBA-BF_4) in ammonia-saturated methanol electrolyte with 0.1 M benzaldehyde initially (see Supplementary Information for details), and electrolysis consisted of passing 2 C of charge at -1.9 V vs. Fc/Fc^+. Products were analysed via NMR as per Supplementary procedure. Glassy carbon (GC) is shown on the top for comparison to a system that is expected to behave via an outer-sphere mechanism. The difference between GC (outer-sphere) and palladium partial currents is over an order of magnitude, as is the difference between platinum and palladium, indicating that the system has a catalyst dependence and is likely following an inner-sphere mechanism. The wide range of Faradaic efficiencies also supports an inner-sphere mechanism.

Specifically, the wide variation in Faradaic efficiencies indicates that differences in partial current are due to differences from interactions with the catalyst materials, not simply differences in the surface area between metal foils. From the partial currents, Ag and Pd are the most active metals for primary amine synthesis, whereas Ag has the highest Faradaic efficiency toward primary amine product compared to all other metals tested.

Partial currents toward other detectable liquid-phase products, namely the secondary amine and coupling product, are also non-zero, but significantly less than the primary amine in most cases. The remaining balance of partial current is likely directed toward hydrogen evolution, discussed broadly and demonstrated explicitly for the case of Ag in the Supplementary Information (Figure S5). These results represent a kinetic analysis in the limit of low conversion (maximum conversion of less than 6% of total substrate in the catholyte), providing an indication of the intrinsic activity of the catalyst toward ERA of benzaldehyde. Low conversion analysis is important for understanding reaction kinetics since both desired and undesired products can build

up over time, altering the system and hindering understanding of the intrinsic reaction kinetics.

Catalyst Reactivity Descriptor

It is typical to justify trends among catalysts for a given reaction using reactant binding energy, as captured by Sabatier's principle.[53] Typically the best catalyst has an intermediate binding energy, and derives its optimal performance from the fact that the reactants are bound strongly enough to the surface so as to exert a catalytic effect, but not so tightly as to poison the catalyst. Sabatier's principle has been applied to diverse reactions including hydrogen evolution[53–55], oxygen evolution[56,57], and carbon dioxide reduction[58,59]. In the case of inner sphere benzylamine synthesis, we would, a priori, expect that the binding energy of some benzylic intermediate or perhaps hydrogen adatoms would provide a reasonable descriptor for catalyst reactivity. Density functional theory (DFT) studies on benzaldehyde adsorption on Pt (a proxy for benzylimine adsorption) have found that benzaldehyde adsorbs primarily via the benzylic ring and that its adsorption energy scales with benzene adsorption energies.[60] Benzene adsorption has been studied with both DFT as well as with experiments, and studies generally focus on two types of systems: (1) coinage metals (Cu, Ag, Au) on which benzene adsorbs weakly; and (2) metals such as platinum and palladium on which benzene adsorbs strongly.[61,62] We find that for our ERA system, benzene adsorption energies do not act as a descriptor (Figure 3, Figure 4, Figure S6); this is evident since palladium and silver have the highest activity, and platinum and gold are among the lowest, indicating that ERA of benzaldehyde is likely not described by the binding energy of a benzylic compound (shown explicitly in Figure S6).

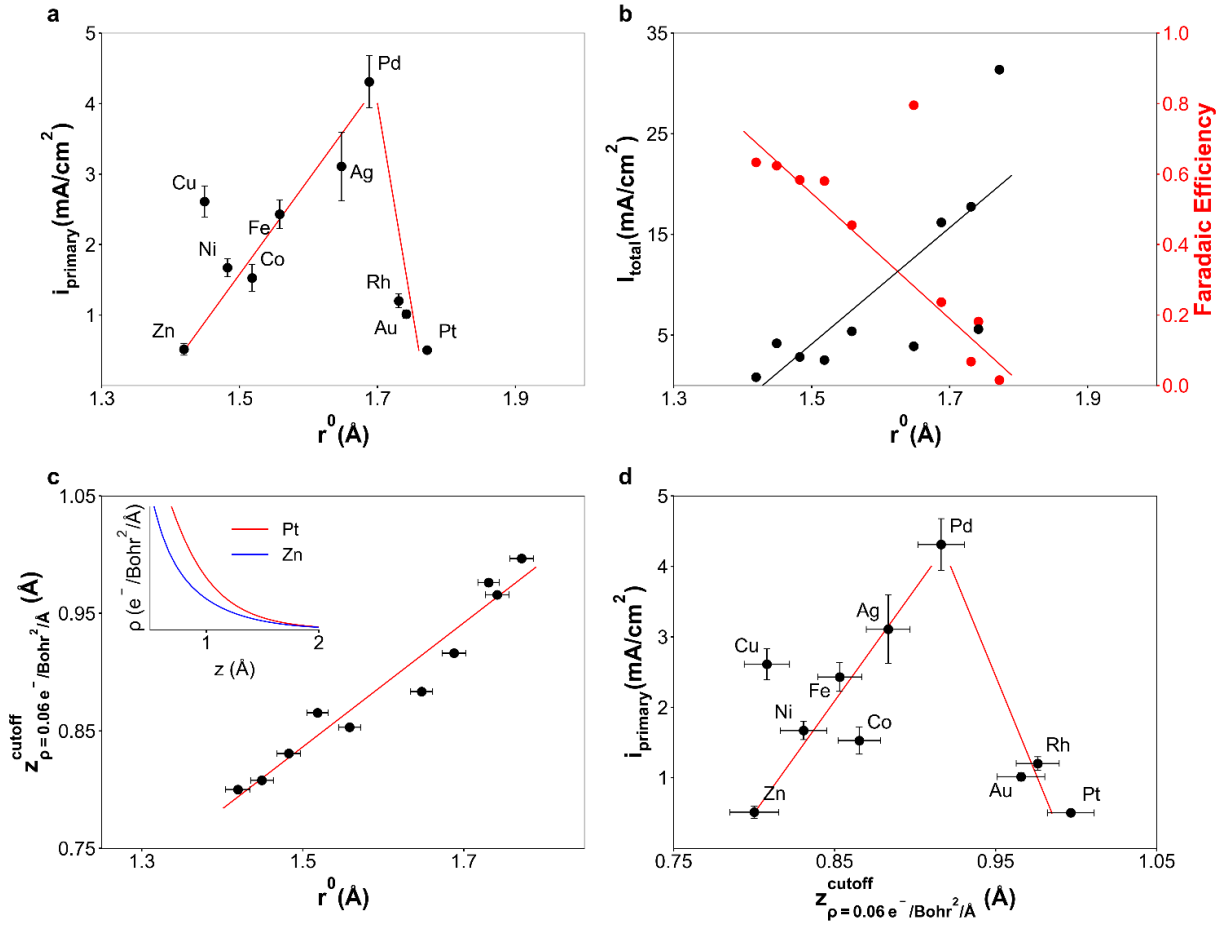

Figure 4. Inner-sphere descriptor for ERA of benzaldehyde. Catalyst reactivity appears to form a volcano-like trend with atomic radius[63–65] as a descriptor (a). In addition, the atomic radius also describes trends in the total current and Faradic efficiencies of the catalysts (b), suggesting that this metal-intrinsic descriptor captures multiple observables of this catalytic system. We use DFT calculations to translate atomic radius to an analogous characteristic length associated with the charge density (electrons per area per unit length in the *z* direction) as a function of distance above a metal surface, defined as $z = 0$ (c). Specifically, the charge decay profile is unique to each metal and follows a roughly exponential decay as a function of height above the surface, a surface-analogue to an atomic radius (c, inset). We find that the distance above the surface at which the charge density decays below 0.06 e^-/Bohr^2/Å above the surface tracks well with atomic radius (c). Correspondingly, the catalyst activity maps neatly onto a characteristic length for the charge density distribution defined by the distance above the surface at which the charge density decays below 0.06 e^-/Bohr^2/Å at ~1 Å above the surface, forming a "volcano" plot with palladium and silver at the top (d). All lines are only to guide the eye. Details on descriptor optimization provided in the ESI. Experimental data points come from Figure 3.

An alternative reactivity descriptor would be hydrogen binding energy since the synthesis of benzylamine requires the addition of two hydrogens to the imine. However, the observed trend in reactivity for ERA of benzaldehyde is not a function of hydrogen binding energy (Figure S6). In

fact, the high reactivity of silver and palladium and the low reactivity of gold and platinum is a rather unique combination that does not scale with any obvious binding energy.[66]

We found that the catalyst reactivity for ERA trends with the atomic radius of the catalyst material, a metal-intrinsic property that is independent of the adsorbate (Figure 4a). Specifically, the reaction rate as a function of atomic radius produces a volcano-like plot. Here, the atomic radius is defined as the location of the charge maximum in the outermost Slater-type orbital of the metal [63–65]. With this observation alone, there remains the possibility that the trend in catalyst reactivity as a function of atomic radius is simply a coincidence. However, when the atomic radius is used to compare catalysts on the basis of total current and Faradaic efficiencies toward the primary amine product, there is an increasing trend in total current as a function of atomic radius and a decreasing trend in Faradaic efficiency as a function of atomic radius (Figure 4b). Combined, these two opposing trends result in a volcano shape for the partial current toward the primary amine. Hence, the atomic radius descriptor captures not just the partial current toward the primary amine but independently captures the total current and Faradaic efficiency.

Although reaction rate does trend with atomic radius, the catalysts in this system are not single atoms but are bulk metal surfaces, so an appropriate method of generalizing the concept of atomic radius to an analogous surface quantity is needed. Fundamentally, the atomic radius is a measure of the radial distribution of charge density in that it is a characteristic length representing the decay of charge density away from the nucleus. A surface descriptor analogous to the atomic radius would be based on analyzing the charge density distribution as a function of position relative to a metal surface.

DFT calculations of metal surfaces enable study of charge density as a function of height relative to the surface. As expected, the charge density decays roughly exponentially away from the surface, defined as $z = 0$, but every metal has a distinct charge density profile (Figure 4c inset, shown for all tested metals in Figure S7). Specifically, the surface charge density for each

metal can be described by a characteristic length, namely the distance above each metal surface, z^{cutoff}, at which the charge density decays below some cutoff charge density, ρ^{cutoff}. This characteristic length, z^{cutoff}, tracks well with the atomic radius when ρ^{cutoff} = 0.06 e^-/Bohr^2/Å (Figure 4c, Supplementary Data Analysis, Figure S8). Accordingly, when using this charge density above the surface as a descriptor, we find a similar volcano trend as that seen using atomic radii (Figure 4d). At cutoff values much smaller or larger, however, the reactivity no longer scales with the charge density (Figure S8). While we have used a cutoff charge density to generate characteristic lengths, the charge density at a fixed point above the surface can also be thought of as being related to an atomic radius; we see that this can also be used as a descriptor of catalyst reactivity (Figure S8). Note that copper is an outlier in this reactivity trend; however, the copper electrode was noticeably altered post-electrolysis, likely due to fast oxidative dissolution in the presence of ammonia that could be coupled with plating at the reductive potential. As a result, the reaction mechanism on copper may be different.

Overall, catalyst reactivity toward ERA of benzaldehyde appears to be well-described by the charge density distribution associated with the catalyst, whether that be the atomic radius or the DFT-calculated charge density distribution, yet the physical rationale for this trend is difficult to discern. Because the DFT-based descriptor is for a metal surface, it could be extended to an arbitrary metal surface (e.g., bimetallic materials, oxides, nitrides, etc.). Such an extension, however, requires knowledge of the exact surface structure—this can be approximated for the simple metals used in this work (Table S6) but can be difficult to accurately acquire for more complex surfaces.

Mechanism Determination

Beyond the influence of the catalyst on the reaction rate, we also studied the mechanism of ERA of benzaldehyde on silver. We chose silver for two reasons: (1) silver was one of the most

active catalysts, and (2) silver had the highest Faradaic efficiency of the studied catalysts.

The Tafel slope can help elucidate the role of voltage in the reaction. Traditionally, the Tafel slope is the slope of the linear region on a plot of voltage versus the logarithm of current, and it reveals information about the role of electrons in the rate-determining step and pre-equilibrium steps. However, recent work has found that a Bayesian interpretation of the Tafel slope over a larger region provides a more accurate and nuanced picture of the role of voltage on the rate-determining step of a reaction.[67] This Bayesian analysis reveals that the mean a posteriori Tafel slope for ERA of benzaldehyde is 100 mV/dec. When combined with a distribution of possible Tafel slopes (Figure 5a inset), the Tafel analysis indicates that the rate-determining step of this reaction is likely the first electron transfer (Figure 5a). Details on the Bayesian Tafel fitting are provided in the Supplementary Data Analysis discussion.

At a range of proton concentrations, the partial current toward the primary amine product remains constant even as the Faradaic efficiency decreases with increasing proton concentration, indicating that protons are not involved in the reaction until after the rate-determining step (Figure 5b). In contrast, at low concentrations of benzaldehyde, the current increases roughly linearly with concentration, but at concentrations greater than ~50 mM, the current and Faradaic efficiency level off and even decrease (Figure 5c). Note that these concentration dependence tests were conducted at -1.74 V vs. Fc/Fc^+, where the reaction is within the Tafel regime (i.e., not limited by mass transport). The partial current toward the primary amine as a function of proton concentration (Figure 5b) and benzaldehyde concentration (Figure 5c) together indicate that the rate-determining step is likely the initial addition of an electron to the benzylimine reactant.

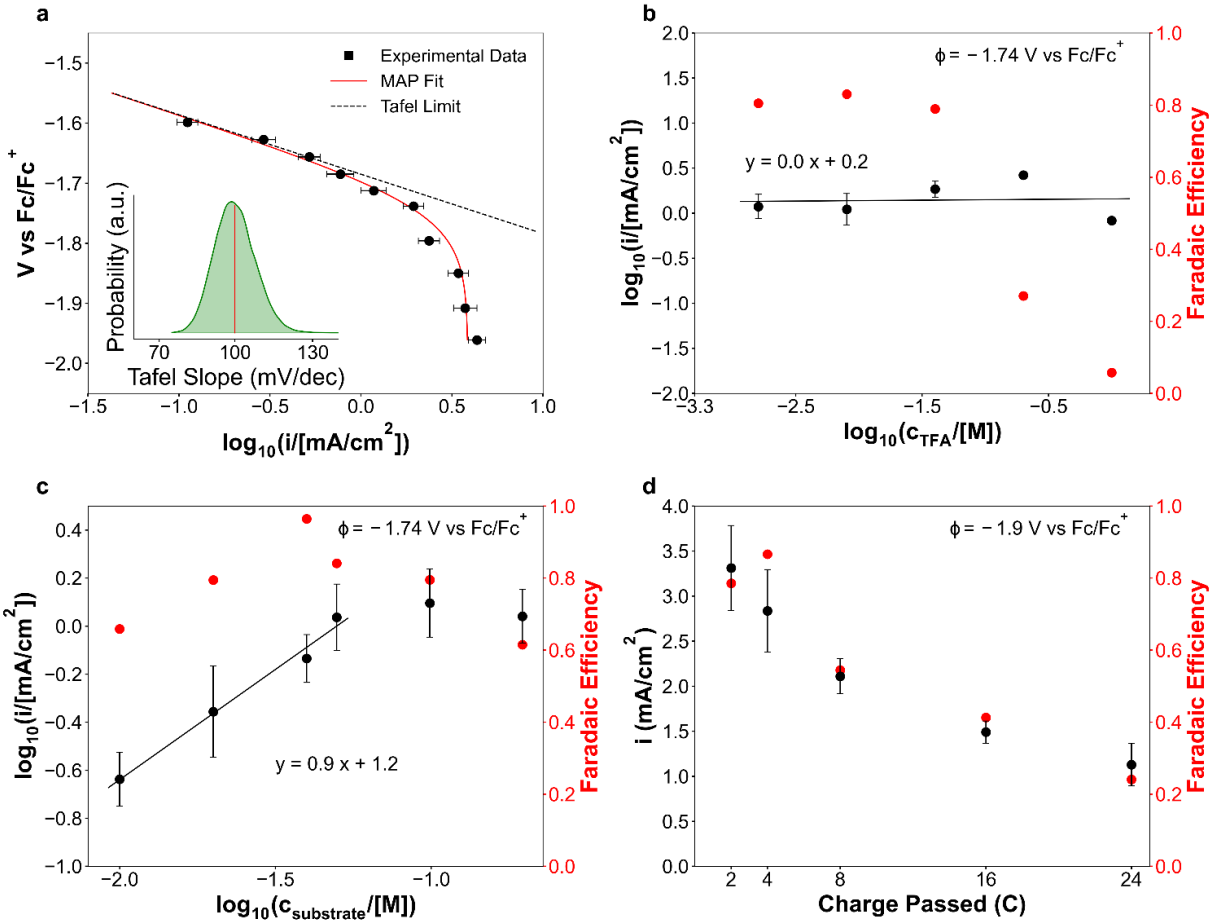

Figure 5. Mechanism determination. A Bayesian Tafel analysis reveals that the first electron transfer is likely the rate-determining step (a). The red line in the Tafel analysis represents the full, holistic fit to the Tafel data using Bayesian statistics, the dashed line represents the linear limit of the Tafel slope, and the inset represents the probability distribution of possible Tafel slopes based on the data with the mean *a posteriori* value (MAP), essentially the expected value of the probability distribution, marked with a red vertical line (a, inset). The reaction rate remains constant as a function of proton concentration at -1.74 V vs. Fc/Fc^+, although the Faradaic efficiency decreases with > 0.1 M concentration of trifluoroacetic acid, likely due to increased hydrogen evolution (b). The partial current as a function of benzaldehyde concentration at -1.74 V vs. Fc/Fc^+ reveals that at low concentrations the reaction is first order in benzaldehyde but that at higher concentrations the reaction rate decreases with increasing benzaldehyde (c). Both the Faradaic efficiency and the partial current toward the primary amine decrease as more coulombs are passed, indicating that something is preventing the reaction from proceeding to completion (d). Time-averaged partial currents and Faradaic efficiencies for various amine products shown in Figures S9-S12. Unless otherwise noted, all reactions were conducted using a 1 M TBA-BF_4 in methanol electrolyte with 0.1 M benzaldehyde and 1 bar of NH_3 initially, and 2 C of charge passed. Primary amine products were quantified via NMR.

The phenomenon of partial currents not scaling with reactant concentration has been observed in previous studies of electrochemical furfural and benzaldehyde reduction at

concentrations above 100 mM.[40,45,49] These studies have postulated that polymerization reactions which are more favorable at higher concentrations can foul the surface and inhibit the desired reductive reaction. The possibility of side reactions that are poisoning the surface is further borne out by the fact that, although the total current remains relatively steady as more coulombs are passed, the average partial current and Faradaic efficiency toward the primary amine decrease (Figure 5d). Note that as the Faradaic efficiency toward amine products decreases, the total current remains roughly constant and the Faradaic efficiency toward hydrogen gas increases at a commensurate rate to balance out the decrease in amine production (Figure S5).

To further investigate the potential poisoning of the catalyst, additional tests were conducted to isolate the problem (Figure S13). In brief, through reuse of foil electrodes and electrolyte solutions, as well as intentional doping of amine products, we found that the species poisoning the catalyst can likely be found in the electrolyte, possibly the result of an undesired side reaction such as polymerization, and it prevents this system from reaching high conversions.

Conclusions

We have shown an electrochemical reductive amination reaction of benzaldehyde and ammonia that relies on voltage instead of high pressures of hydrogen gas and elevated temperatures to drive the reaction. In addition, this reaction proceeds via an inner-sphere mechanism, in contrast to previous ERA studies which generally describe outer-sphere reactions. Using DFT, we developed a metal-intrinsic descriptor that shows that catalyst activity is a function of the charge density above the reaction surface. On a silver foil, found to be among the most active and selective for ERA of benzaldehyde, the rate-determining step is likely the first electron transfer to the benzylimine substrate. The conversion of the reaction is currently limited by a fouling mechanism that causes the Faradaic efficiency and partial current to decrease as more coulombs are passed. The poisoning is attributed to a species that accumulates in the electrolyte as

opposed to solely from changes of the electrode itself. This system advances the use of heterogeneous electrocatalysts for reductive amination, opening up a large phase space of electrocatalysts that can direct selectivity and drive the reaction without the need for pressurization.

Materials and Methods

Additional details and comprehensive discussion of all materials and procedures are available in the ESI.

Electrochemical Experiments

The electrolyte consisted of 1 M tetrabutylammonium tetrafluoroborate in anhydrous methanol, saturated with 1 bar of ammonia. After the addition of benzaldehyde, the electrolyte was sealed and stored in the dark overnight. Electrochemical experiments were conducted after the solutions equilibrated in a two compartment PEEK cell with a Celgard separator. A leak-free Ag/AgCl reference (Innovative Instruments, LF-2) was used as a pseudo-reference and calibrated against ~5 mM Fc/Fc^+ each day. The anode was always a platinum foil, and the cathode electrode foils were various metals, polished with 400 grit sandpaper before each usage. All electrochemical experiments were performed using a Biologic VMP3 potentiostat. In general, each experiment consisted of a constant potential hold until 2 coulombs were passed.

Product Quantification

After each electrochemical experiment, the cell was rinsed with 0.5 mL of methanol in each compartment and the solvent was removed from the resulting mixture using a rotary evaporator.

A solution of 0.5 M HCl in D_2O was then added with 10 μmol of DMSO. Liquid products were quantified with a Bruker Avance Neo NMR machine at 500 MHz using solvent suppression (Figures S3 and Supplementary Product Analysis section). Hydrogen quantification was done with an SRI gas chromatograph while bubbling Ar gas at 5 standard cubic centimetres per minutes through the catholyte (Figure S5 shows quantification curves).

Density Functional Theory

All DFT calculation were done with the Quantum Espresso[68–70]. electronic structure code using PAW type PBE functional[71–73]. Details on the input parameters are available in the ESI. Slabs were 4 layers with the bottom two layers frozen during atomic position relaxation. Spin-polarized calculations were used for ferromagnetic metals, namely Fe, Co, and Ni, with the magnetic moments allowed to converge during optimization. The environ module of Quantum Espresso was used to include implicit solvation in the slab calculations.

Data Availability

All raw data and analysis scripts will be available upon request to the corresponding author.

Acknowledgments

This material is based on work supported by the National Science Foundation under Grant No. 1944007. The authors thank Nathan Corbin, Nikifar Lazouski, and Kindle Williams for useful discussions. The authors also thank Andrew Medford, Ben Comer, Robert Warburton, and Aditya Nandy for help with DFT. ZJS and KS also acknowledges a graduate research fellowship from the National Science Foundation under Grant No. 1745302. ZJS acknowledges funding from Chevron through the MIT Energy Initiative. The authors acknowledge the MIT SuperCloud and

Lincoln Laboratory Supercomputing Center for providing HPC resources that have contributed to the research results reported within this paper.

Author Contributions

Conceptualization, Z.J.S. and K.M.; Resources, Z.J.S. and K.M.; Data curation, Z.J.S.; Software, Z.J.S.; Formal Analysis, Z.J.S.; Supervision, Z.J.S. and K.M.; Funding acquisition, Z.J.S. and K.M.; Validation, Z.J.S. and M.C.; Investigation, Z.J.S.; Visualization, Z.J.S.; Methodology, Z.J.S. and K.M.; Writing – original draft, Z.J.S.; Writing – review & editing, Z.J.S., M.C., K.S., K.M.; Project administration, Z.J.S. and K.M.

Competing Interest Statement

There are no competing interests to declare.

References

1. IEA, ICCA & DECHEMA. *Technology Roadmap: Energy and GHG Reductions in the Chemical Industry via Catalytic Processes*. (2013).

2. Jiao, F. & Xu, B. Electrochemical Ammonia Synthesis and Ammonia Fuel Cells. *Advanced Materials* **31**, 1–5 (2019).

3. Nørskov, J. *et al. Sustainable Ammonia Synthesis*. (2016).

4. Lazouski, N., Schiffer, Z. J., Williams, K. & Manthiram, K. Understanding Continuous Lithium-Mediated Electrochemical Nitrogen Reduction. *Joule* **3**, 1127–1139 (2019).

5. van Geem, K. M., Galvita, V. V. & Marin, G. B. Making chemicals with electricity. *Science* **364**, 734–735 (2019).

6. Gu, S., Xu, B. & Yan, Y. Electrochemical Energy Engineering: A New Frontier of Chemical Engineering Innovation. *Annual Review of Chemical and Biomolecular Engineering* **5**, 429–454 (2014).

7. Schiffer, Z. J. & Manthiram, K. Electrification and Decarbonization of the Chemical Industry. *Joule* **1**, 10–14 (2017).

8. Botte, G. G. Electrochemical Manufacturing in the Chemical Industry. *Interface magazine* **23**, 49–55 (2014).

9. Schiffer, Z. J., Limaye, A. M. & Manthiram, K. Thermodynamic Discrimination between Energy Sources for Chemical Reactions. *Joule* **5**, 135–148 (2021).

10. Afanasyev, O. I., Kuchuk, E., Usanov, D. L. & Chusov, D. Reductive Amination in the Synthesis of Pharmaceuticals. *Chemical Reviews* **119**, 11857–11911 (2019).

11. Podyacheva, E., Afanasyev, O. I., Tsygankov, A. A., Makarova, M. & Chusov, D. Hitchhiker's Guide to Reductive Amination. *Synthesis (Germany)* **51**, 2667–2677 (2019).

12. Gomez, S., Peters, J. A. & Maschmeyer, T. The Reductive Amination of Aldehydes and Ketones and the Hydrogenation of Nitriles: Mechanistic Aspects and Selectivity Control. *Advanced Synthesis and Catalysis* **344**, 1037–1057 (2002).

13. Liang, G. *et al.* Production of Primary Amines by Reductive Amination of Biomass-Derived Aldehydes/Ketones. *Angewandte Chemie - International Edition* **56**, 3050–3054 (2017).

14. Irrgang, T. & Kempe, R. Transition-metal-catalyzed reductive amination employing hydrogen. *Chemical Reviews* **120**, 9583–9674 (2020).

15. Murugesan, K. *et al.* Catalytic reductive aminations using molecular hydrogen for synthesis of different kinds of amines. *Chemical Society Reviews* **49**, 6273–6328 (2020).

16. Senthamarai, T. *et al.* Simple ruthenium-catalyzed reductive amination enables the synthesis of a broad range of primary amines. *Nature Communications* 1–12 (2018) doi:10.1038/s41467-018-06416-6.

17. Gross, T., Seayad, A. M., Ahmad, M. & Beller, M. Synthesis of Primary Amines: First Homogeneously Catalyzed Reductive Amination with Ammonia. *Organic Letters* **4**, 2055–2058 (2002).

18. Abdel-Magid, A. F., Carson, K. G., Harris, B. D., Maryanoff, C. A. & Shah, R. D. Reductive Amination of Aldehydes and Ketones with Sodium Triacetoxyborohydride. Studies on Direct and Indirect Reductive Amination Procedures [1]. *The Journal of Organic Chemistry* **61**, 3849–3862 (1996).

19. BASF. Benzylamine. *Products* https://products.basf.com/global/en/ci/benzylamine.html (2021).

20. Lutz Heuer. Benzylamine. in *Ullmann's Encyclopedia of Industrial Chemistry, Vol. 5* 385–387 (2012). doi:10.1002/14356007.a04.

21. Jagadeesh, R. V. *et al.* MOF-derived cobalt nanoparticles catalyze a general synthesis of amines. *Science* **358**, 326–332 (2017).

22. Hahn, G., Kunnas, P., de Jonge, N. & Kempe, R. General synthesis of primary amines via reductive amination employing a reusable nickel catalyst. *Nature Catalysis* **2**, 71–77 (2019).

23. Jv, X. *et al.* Efficient and Mild Reductive Amination of Carbonyl Compounds Catalyzed by Dual-Function Palladium Nanoparticles. *ACS Sustainable Chemistry and Engineering* **8**, 1618–1626 (2020).

24. Root, D. K. & Smith, W. H. Electrochemical Behavior of Selected Imine Derivatives , Reductive Carboxylation , s-Amino Acid Synthesis. *Journal of The Electrochemical Society* **129**, 1231–1236 (1982).

25. Zuman, P. Polarographic Behaviour of Acetone. *Nature* 485–486 (1950).

26. Zuman, P. & Exner, O. Oxime derivatives. VIII. Polarographic Reduction of O- and N-Substituted Oximes. *Collection Czechoslovakian Chemical Sommunications* **28**, 1832–1852 (1963).

27. Benson, H. G. & Scott, J. M. W. Polarographic reduction of some Schiff bases in dimethylformamide. Part II. Some further theoretical considerations. *Canadian Journal of Chemistry* **46**, 2895 (1968).

28. Andrieux, C. P. & Saveant, J. M. Dimerization, Disproportionation and E.C.E. Mechanisms in the Reduction of Imines in Acetonitrile and Dimethylformamide. *Electroanalytical Chemistry and Interfacial Electrochemistry* **33**, 453–461 (1971).

29. Isse, A. A., Abdurahman, A. M. & Vianello, E. Role of proton transfer in the electrochemical reduction mechanism of salicylideneaniline. *Journal of Electroanalytical Chemistry* **431**, 249–255 (1997).

30. Fry, A. J. & Reed, R. G. The Electrochemical Reduction of Imines in Dimethylformamide. *Journal of the American Chemical Society* **91**, 6448–6451 (1969).

31. Chiba, T., Okimoto, M., Nagai, H. & Takata, Y. Electrocatalytic Reduciton Using Raney Nickel. *Bulletin of the Chemical Society of Japan* **56**, 719–723 (1983).

32. Scott, J. M. W. & Jura, W. H. Polarographic reduction of some schiff bases in dimethylformamide. *Canadian Journal of Chemistry* **45**, 2375 (1967).

33. Roylance, J. J. & Choi, K. S. Electrochemical reductive amination of furfural-based biomass intermediates. *Green Chemistry* **18**, 5412–5417 (2016).

34. Blanco, D. E., Dookhith, A. Z. & Modestino, M. A. Controlling Selectivity in the Electrocatalytic Hydrogenation of Adiponitrile through Electrolyte Design. *ACS Sustainable Chemistry & Engineering* **8**, 9027–9034 (2020).

35. Zhao, Y., Liu, C., Wang, C., Chong, X. & Zhang, B. Sulfur vacancy-promoted highly selective electrosynthesis of functionalized aminoarenes via transfer hydrogenation of nitroarenes with H2O over a Co3S4−x nanosheet cathode. *CCS Chemistry* **3**, 507–515 (2021).

36. Schmickler, W. & Santos, E. Theoretical considerations of electron-transfer reactions. in *Interfacial Electrochemistry* (eds. Schmickler, W. & Santos, E.) 99–115 (Springer Berlin Heidelberg, 2010). doi:10.1007/978-3-642-04937-8_10.

37. Bondue, C. J. & Koper, M. T. M. M. A mechanistic investigation on the electrocatalytic reduction of aliphatic ketones at platinum. *Journal of Catalysis* **369**, 302–311 (2019).

38. Polcaro, A. M., Palmas, S. & Dernini, S. Role of Catalyst Characteristics in Electrocatalytic Hydrogenation : Reduction of Benzaldehyde and Acetophenone on Carbon Felt / Pd Electrodes. 1315–1322 (1993) doi:10.1021/ie00019a005.

39. Song, Y. *et al.* Hydrogenation of benzaldehyde via electrocatalysis and thermal catalysis on carbon-supported metals. *Journal of Catalysis* **359**, 68–75 (2018).

40. Anibal, J. & Xu, B. Electroreductive C-C Coupling of Furfural and Benzaldehyde on Cu and Pb Surfaces. *ACS Catalysis* **10**, 11643–11653 (2020).

41. Zuman, P. Aspects of Electrochemical Behavior of Aldehydes and Ketones in Protic Media. *Electroanalysis* **18**, 131–140 (2006).

42. Bondue, C. J. & Koper, M. T. M. Electrochemical Reduction of the Carbonyl Functional Group: The Importance of Adsorption Geometry, Molecular Structure, and Electrode Surface Structure. (2019) doi:10.1021/jacs.9b05397.

43. Bondue, C. J., Calle-vallejo, F., Figueiredo, M. C. & Koper, M. T. M. Structural principles to steer the selectivity of the electrocatalytic reduction of aliphatic ketones on platinum. *Nature Catalysis* **2**, (2019).

44. Chadderdon, X. H. *et al.* Mechanisms of Furfural Reduction on Metal Electrodes: Distinguishing Pathways for Selective Hydrogenation of Bioderived Oxygenates. *Journal of the American Chemical Society* **139**, 14120–14128 (2017).

45. May, A. S. & Biddinger, E. J. Strategies to Control Electrochemical Hydrogenation and Hydrogenolysis of Furfural and Minimize Undesired Side Reactions. *ACS Catalysis* **10**, 3212–3221 (2020).

46. Akhade, S. A. *et al.* Electrocatalytic hydrogenation of biomass-derived organics: A review. *Chemical Reviews* **120**, 11370–11419 (2020).

47. Jung, S. & Biddinger, E. J. Electrocatalytic Hydrogenation and Hydrogenolysis of Furfural and the Impact of Homogeneous Side Reactions of Furanic Compounds in Acidic Electrolytes. *ACS Sustainable Chemistry and Engineering* **4**, 6500–6508 (2016).

48. Jung, S., Karaiskakis, A. N. & Biddinger, E. J. Enhanced activity for electrochemical hydrogenation and hydrogenolysis of furfural to biofuel using electrodeposited Cu catalysts. *Catalysis Today* **323**, 26–34 (2019).

49. Jung, S. & Biddinger, E. J. Controlling Competitive Side Reactions in the Electrochemical Upgrading of Furfural to Biofuel. *Energy Technology* **6**, 1370–1379 (2018).

50. Lopez-Ruiz, J. A. *et al.* Understanding the Role of Metal and Molecular Structure on the Electrocatalytic Hydrogenation of Oxygenated Organic Compounds. *ACS Catalysis* 9964–9972 (2019) doi:10.1021/acscatal.9b02921.

51. Krupka, J., Dluhos, L. & Mro, L. Evaluation of Benzylamine Production via Reductive Amination of Benzaldehyde in a Slurry Reactor. *Chemical Engineering & Technology* 870–877 (2017) doi:10.1002/ceat.201600538.

52. Noviandri, I. *et al.* The Decamethylferrocenium/Decamethylferrocene Redox Couple: A Superior Redox Standard to the Ferrocenium/Ferrocene Redox Couple for Studying Solvent Effects on the Thermodynamics of Electron Transfer. *Journal of Physical Chemistry B* **103**, 6713–6722 (1999).

53. Nørskov, J. K. *et al.* Trends in the Exchange Current for Hydrogen Evolution. *Journal of The Electrochemical Society* **152**, J23 (2005).

54. Laursen, A. B. *et al.* Electrochemical hydrogen evolution: Sabatiers principle and the volcano plot. *Journal of Chemical Education* **89**, 1595–1599 (2012).

55. Sheng, W. *et al.* Correlating hydrogen oxidation and evolution activity on platinum at different pH with measured hydrogen binding energy. *Nature Communications* **6**, 5848 (2015).

56. Man, I. C. *et al.* Universality in Oxygen Evolution Electrocatalysis on Oxide Surfaces. *ChemCatChem* **3**, 1159–1165 (2011).

57. Mom, R. V., Cheng, J., Koper, M. T. M. & Sprik, M. Modeling the oxygen evolution reaction on metal oxides: The infuence of unrestricted DFT calculations. *Journal of Physical Chemistry C* **118**, 4095–4102 (2014).

58. Feaster, J. T. *et al.* Understanding Selectivity for the Electrochemical Reduction of Carbon Dioxide to Formic Acid and Carbon Monoxide on Metal Electrodes. *ACS Catalysis* **7**, 4822–4827 (2017).

59. Liu, X. *et al.* Understanding trends in electrochemical carbon dioxide reduction rates. *Nature Communications* **8**, 1–7 (2017).

60. Rasmussen, A. M. H. & Hammer, B. Adsorption, mobility, and dimerization of benzaldehyde on Pt(111). *Journal of Chemical Physics* **136**, (2012).

61. Silbaugh, T. L. & Campbell, C. T. Energies of formation reactions measured for adsorbates on late transition metal surfaces. *Journal of Physical Chemistry C* **120**, 25161–25172 (2016).

62. Liu, W. *et al.* Structure and energetics of benzene adsorbed on transition-metal surfaces: Density-functional theory with van der Waals interactions including collective substrate response. *New Journal of Physics* **15**, (2013).

63. Clementi, E., Raimondi, D. L. & Reinhardt, W. P. Atomic screening constants from SCF functions. II. Atoms with 37 to 86 electrons. *The Journal of Chemical Physics* **47**, 1300–1307 (1967).

64. Clementi, E. & Raimondi, D. L. Atomic screening constants from SCF functions. *The Journal of Chemical Physics* **38**, 2686–2689 (1963).

65. Ghosh, D. C. & Biswas, R. Theoretical calculation of absolute radii of atoms and ions. Part 1. Theatomic radii. *International Journal of Molecular Sciences* **3**, 87–113 (2002).

66. Schmidt, P. S. & Thygesen, K. S. Benchmark Database of Transition Metal Surface and Adsorption Energies from Many-Body Perturbation Theory. *Journal of Physical Chemistry C* **122**, 4381–4390 (2018).

67. Limaye, A. M., Zeng, J. S., Willard, A. P. & Manthiram, K. Bayesian data analysis reveals no preference for cardinal Tafel slopes in CO2 reduction electrocatalysis. *Nature Communications* **12**, 1–10 (2021).

68. Giannozzi, P. *et al.* Advanced capabilities for materials modelling with QUANTUM ESPRESSO. *Journal of Physics: Condensed Matter* **29**, 465901 (2017).

69. Giannozzi, P. *et al.* QUANTUM ESPRESSO: a modular and open-source software project for quantum simulations of materials. *Journal of Physics: Condensed Matter* **21**, 395502 (19pp) (2009).

70. Giannozzi, P. *et al.* Quantum ESPRESSO toward the exascale. *The Journal of Chemical Physics* **152**, 154105 (2020).

71. Vanderbilt, D. Soft self-consistent pseudopotentials in a generalized eigenvalue formalism. *Physical Review B* **41**, 7892–7895 (1990).

72. Blöchl, P. E. Projector augmented-wave method. *Physical Review B* **50**, 17953–17979 (1994).

73. Dal Corso, A. Pseudopotentials periodic table: From H to Pu. *Computational Materials Science* **95**, 337–350 (2014).